Preferential formation of highly efficient Eu luminescent centers in Eu-doped GaN grown on semipolar (20$\bar{2}$1) GaN

A. Takeo,[1] S. Ichikawa,[1,2] D. Timmerman,[1] J. Tatebayashi,[1] and Y. Fujiwara[1,3,4,5]

[1)] *Graduate School of Engineering, The University of Osaka, 2-1 Yamadaoka, Suita, Osaka 565-0871, Japan*

[2)] *Research Center for Ultra-High Voltage Electron Microscopy, The University of Osaka, Ibaraki, Osaka, 567-0047, Japan*

[3)] *Research Organization of Science and Technology, Ritsumeikan University, 1-1-1 Noji-higashi, Kusatsu, Shiga 525-8577 Japan*

[4)] *Institute for Scientific and Industrial Research, The University of Osaka, 8-1 Mihogaoka, Ibaraki, Osaka 567-0047, Japan*

[5)] *R^3 Institute of Newly-Emerging Science Design, The University of Osaka, 1-3 Machikaneyama, Toyonaka, Osaka 560-8531, Japan*

(*Electronic mail: ichikawa.shuhei.eei.eng@osaka-u.ac.jp)

(Dated: 28 February 2026)

Eu-doped GaN (GaN:Eu) exhibiting bright red emission is a promising material for the realization of ultrahigh-resolution micro-LED displays that can be applied to virtual reality/augmented reality/mixed reality (VR/AR/MR). The full-color monolithic integration of a red GaN:Eu LED and blue/green InGaN LEDs is a key technology, in which the use of semipolar substrates is preferred to suppress wavelength shift in the InGaN LEDs under current injections. We investigate the effects of the growth plane on GaN:Eu-based red emission and find that the emission intensity from a semipolar (20$\bar{2}$1) GaN:Eu is drastically enhanced as compared with a conventional (0001) GaN:Eu,O. Combined excitation-emission spectroscopy reveal that the fraction of Eu luminescent centers with different local structures dramatically changed. A highly efficient Eu center is preferentially formed and its abundance increases by more than two orders. These results show a clear pathway to develop a red LED with higher light output power.

GaN and the related alloys can cover a wide range of bandgaps and have been developed for various optical devices[1–4]. To date, efficient blue and green light-emitting diodes (LEDs) have been fabricated by adjusting the indium composition of InGaN quantum wells (QWs)[5,6], and the efficient red LEDs based on the III-nitride material system is required to realize the monolithic integration towards next-generation micro-LED displays with ultrahigh resolution[7–10]. However, InGaN QWs with high indium compositions suffer from various issues, such as low crystalline quality and strong internal electric fields in the well layers[11–14]. Recently, InGaN-based red LEDs with high external quantum efficiency (EQE) beyond several percents or approaching 10% have intensively been developed[15,16], and the micro-LEDs have been demonstrated[17–19]. For micro-LEDs, the efficiency is affected by not only the material quality but also the size effect due to surface recombination attributed to sidewall damage. The size effect has been investigated significantly and methods have been proposed to address this issue[17,20,21]. Furthermore, the wavelength shift induced by screening of the internal electric field with current injections is still challenging in InGaN QWs towards display applications[22].

Eu-doped GaN (GaN:Eu) is a promising material to overcome these problems, and we have reported the first demonstration of a GaN:Eu-based red LED[23]. The GaN:Eu-based red LEDs have exhibited narrow line-widths and stable emission wavelengths under current injections due to the intra-4f shell transitions ($^5D_0$–$^7F_2$) in Eu^{3+} ions. We have achieved a light output power of 1.25 mW at 20 mA operation and the maximum EQE of 9% at 2 mA[24]. The suppressed carrier diffusion in Eu-doped layers can decrease surface recombination paths at the side-walls in micro-LED structures[25], which is a key technology to realize small-size, ultrahigh-resolution displays. In addition, we have demonstrated full-color monolithic integration of the GaN:Eu-based red LED and blue/green InGaN LEDs showing an exceptionally wide color gamut[10]. However, the color gamut of full-color LEDs decreased under high current injection levels due to the wavelength shift of InGaN-based green LEDs induced by the screening of the internal electric fields. One of the techniques to suppress the wavelength shift is the utilization of semipolar plane substrates.

One of the factors that determine the luminescence intensity of Eu^{3+} ions under current injection is the energy transfer efficiency from the GaN host to Eu^{3+} ions. The emission spectrum of GaN:Eu has several peaks around 620 nm corresponding to the $^5D_0$–$^7F_2$ transitions, which ascribed to the existence of several luminescent centers with different local environments. In our previous work, eight unique Eu^{3+} luminescent centers, which is labeled OMVPE1 to OMVPE8, have been observed in GaN:Eu grown by organometallic vapor-phase epitaxy (OMVPE)[26]. Generally, the energy transfer efficiency strongly depends on the local environment around Eu^{3+} ions, and it is necessary to increase the concentration of efficient luminescent centers to obtain higher light output powers in GaN:Eu-based red LEDs. In particular, the luminescent center labeled OMVPE7 shows the highest energy transfer efficiency from the GaN host[27], having an excitation cross-section two orders of magnitude larger than other centers under current injection[28]. The impurity co-doping technique is an effective method to control the distribution of luminescent centers. For example, Er-doped GaAs shows a remarkable increase of

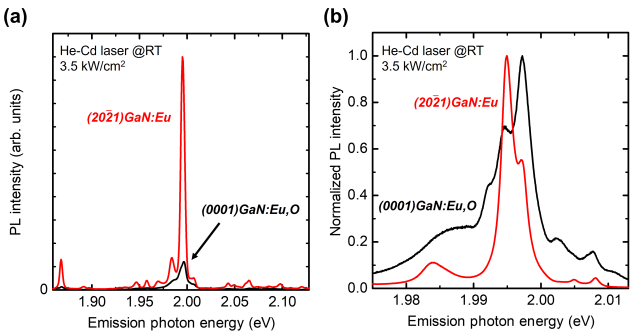

FIG. 1. (a) PL spectra of (20$\bar{2}$1) GaN:Eu and conventional (0001) GaN:Eu,O. (b) Normalized PL spectra at each peak intensities of (20$\bar{2}$1) GaN:Eu and conventional (0001) GaN:Eu,O.

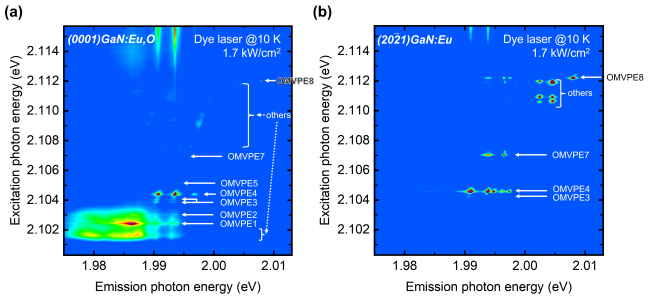

FIG. 2. CEES mapping images of (a) conventional (0001) GaN:Eu,O and (b) (20$\bar{2}$1) GaN:Eu.

emission intensity due to selective formation of luminescent centers by intentional co-doping of oxygen[29]. In the case of GaN:Eu, co-doping of various impurities such as O, Mg and Si has been reported[30]. Co-doping of Eu and O during the crystal growth allows to increase the distribution of OMVPE7 because the local environment is related to oxygen substituting Ga sites[31,32]. However, the oxygen concentration in conventional (0001) Eu,O-codoped GaN (GaN:Eu,O) is currently limited up to 2.5% of the Eu concentration, and most of the Eu^{3+} ions form inefficient centers[32].

The impurity incorporation depends on the growth conditions, such as growth temperature and reactor pressure. Typically, low temperature growth facilitates oxygen incorporation into GaN[33]. However, low temperature growth simultaneously decreases optical properties due to the degradation of crystal quality and the reduction of Eu incorporation[34]. The utilization of a different crystal orientation is another approach which changes the impurity incorporation even under the same growth temperature[35–39]. Several groups have reported that the semipolar planes such as (20$\bar{2}$1), (10$\bar{1}$1), and (11$\bar{2}$2) promote oxygen incorporation as compared to the (0001) GaN growth[35,38]. In this paper, we investigate the effects of crystal orientation and the impurity incorporation on Eu luminescent centers when the semipolar (20$\bar{2}$1) GaN template on sapphire is used for GaN:Eu growth.

Samples were grown on commercially available semipolar (20$\bar{2}$1) GaN templates, which were grown on (22$\bar{4}$1) patterned sapphire substrates using the OMVPE method. Trimethylgallium and ammonia (NH_3) were used as the precursors for GaN growth, and Eu was doped using bis(npropyltetramethylcyclopentadienyl)europium ($EuCp_2^{pm}$). After the initial growth of a 2-μm-thick undoped-GaN layer, a 400-nm-thick GaN:Eu layer was subsequently grown at 900°C. The Eu concentration was 5.6×10^{19} cm^{-3}, as determined by secondary ion mass spectrometry (SIMS) measurement. For comparison, a GaN:Eu,O sample was grown on a (0001) sapphire substrate with conventional growth conditions. The growth was initiated with the formation of a low-temperature GaN buffer layer at 470°C and a 1.5-μm-thick undoped-GaN layer, followed by a 400-nm-thick GaN:Eu,O layer at 960°C. The Eu concentration was determined to be 5.8×10^{19} cm^{-3}. These samples were grown at 100 kPa, and the growth temperature of the Eu-doped layers was optimized to maximize the photoluminescence (PL) intensity of Eu^{3+} emission under above bandgap excitation.

PL measurements were performed using a He-Cd laser (λ_{exc} = 325 nm) for above bandgap excitation, where Eu^{3+} ions were excited through the energy transfer from the GaN host to Eu^{3+} ions. In addition, combined excitation-emission spectroscopy (CEES) was performed to distinguish each Eu luminescent center using a tunable dye laser (λ_{exc} = 586–589 nm) for resonant excitation of Eu^{3+} ions. In the CEES measurements, Eu^{3+} ions were excited from the $^7F_0$ to the $^5D_0$ states, which do not split by the crystal field and have unique excitation energies for the respective Eu^{3+} luminescent centers because they are perturbated by their local environments. Thus, the emission from each luminescent center can be obtained by tuning the excitation wavelength in small steps. The CEES measurements were performed at 10 K in a closed-cycle helium cryostat in order to isolate the emission from each luminescent center.

Time-resolved PL (TR-PL) measurements were also performed under resonant excitations using the dye laser modulated with an acousto-optic modulator. The luminescence was dispersed by a 50 cm focal length spectrometer and detected by a photomultiplier tube.

First of all, in order to compare the luminescence properties between (20$\bar{2}$1) GaN:Eu and conventional (0001) GaN:Eu,O, PL measurements under above bandgap excitation were performed at room temperature (RT). Figure 1(a) shows PL spectra of the both samples. The emission peaks associated with the intra-4f shell transitions of Eu^{3+} ions were observed. The dominant luminescence peaks from 1.971 to 2.016 eV were assigned to the $^5D_0$–$^7F_2$ transitions in Eu^{3+} ions. Although the Eu concentration was almost the same for the both samples, the integrated PL intensity of (20$\bar{2}$1) GaN:Eu was more than 3.6 times as high as that of (0001) GaN:Eu,O. It suggests that an improvement of the energy transfer efficiency from GaN host to Eu^{3+} ions in (20$\bar{2}$1) GaN:Eu. PL spectra normalized at the peak intensities are shown in Fig. 1(b). It was found that the spectral shape of (20$\bar{2}$1) GaN:Eu dramatically changed from that of the conventional (0001) GaN:Eu,O, and it exhibited a narrow line-width with a full width at half maximum of 4.0 meV, whereas that of (0001) GaN:Eu,O was 6.0 meV. Therefore, the origin of the PL enhancement in (20$\bar{2}$1)

TABLE I. Excitation photon energy, rise time and decay time for each luminescent center in $(20\bar{2}1)$ GaN:Eu and (0001) GaN:Eu,O under resonant excitation.

Eu center i	$(20\bar{2}1)$ GaN:Eu			(0001) GaN:Eu,O		
	E_{exc} (eV)	$\tau_{\mathrm{rise},i}$ (μs)	$\tau_{\mathrm{decay},i}$ (μs)	E_{exc} (eV)	$\tau_{\mathrm{rise},i}$ (μs)	$\tau_{\mathrm{decay},i}$ (μs)
1	–	–	–	2.1024	213	238
2	–	–	–	2.1030	218	230
3	2.1042	149	242	2.1038, 2.1040	210	269
4	2.1046	191	246	2.1044	270	290
5	–	–	–	2.1051	162	267
7	2.1070	159	223	2.1069	184	227
8	2.1122	156	227	2.1120	169	207

GaN:Eu was not an increase of the light extraction efficiency but a change in variation of luminescent centers.

To elucidate the origin of spectral differences in detail, CEES measurements were performed. Figures 2(a) and (b) show CEES mapping results for (0001) GaN:Eu,O and $(20\bar{2}1)$ GaN:Eu, respectively. Although various types of luminescent centers were detected in the both samples, the distributions were significantly different. The luminescent centers designated as OMVPE1, OMVPE2 and OMVPE4 were dominantly observed in the (0001) GaN:Eu,O at the resonant excitation photon energies (E_{exc}) of 2.1024, 2,1030 and 2.1044 eV, respectively[26], whereas the OMVPE1 and OMVPE2 were absent in the $(20\bar{2}1)$ GaN:Eu. Typically, a coupled pair of OMVPE1 and OMVPE2 is ascribed to clusters of Eu atoms[26], and they show broad emissions with low efficiency. Thus, Eu clusters were well suppressed in the $(20\bar{2}1)$ GaN:Eu, resulting in the narrow PL line-width under above bandgap excitation as shown in Fig. 1(b).

In the $(20\bar{2}1)$ GaN:Eu, OMVPE4, OMVPE7 and OMVPE8, at E_{exc} of 2.1046, 2.1070 and 2.1122 eV, respectively, were detected as dominant luminescent centers. The luminescent centers and the E_{exc} in each sample were listed in Tab. I. The slight difference of the resonant excitation energy of 0.1–0.2 meV between the (0001) GaN:Eu,O and $(20\bar{2}1)$ GaN:Eu is caused by differences in the local strain environment. Eu^{3+} ions substituting Ga sites (Eu_{Ga}) induce compressive strain in a GaN:Eu layer due to the difference in atomic sizes, and it affects the energy shift in intra-4f shell transitions[40,41]. In semipolar plane GaN, the strain occurs so that the projections of reciprocal lattice vectors of unstrained GaN and strained GaN:Eu on the interface agrees, and the induced compressive strain in $(20\bar{2}1)$ GaN:Eu should be different from (0001) GaN:Eu,O[42,43]. In addition to the energy shifts in $^7F_0$–$^5D_0$ excitations, we also confirmed the energy difference of $\sim$0.2 meV in the PL peaks, originating from the $^5D_0$–$^7F_2$ transitions of the Eu centers, between the samples.

From the CEES results, we calculated the concentration of each luminescent center. Under resonant excitation conditions, the excited Eu concentration of each luminescent center is given by the following rate equation[44],

$$\frac{\mathrm{d}N^*_{\mathrm{Eu},i}}{\mathrm{d}t} = \sigma_i\phi\left(N_{\mathrm{Eu},i} - N^*_{\mathrm{Eu},i}\right) - \frac{N^*_{\mathrm{Eu},i}}{\tau_{\mathrm{decay},i}}, \tag{1}$$

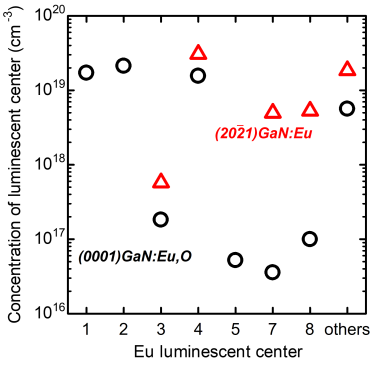

FIG. 3. Concentration of Eu luminescent centers of $(20\bar{2}1)$ GaN:Eu and (0001) GaN:Eu,O.

where i and ϕ denote the labeled numbers of Eu centers (1–8) and photon flux, respectively. $N_{\mathrm{Eu},i}$ and $N^*_{\mathrm{Eu},i}$ indicate the concentrations of each Eu^{3+} center and the excited amount, respectively. $\tau_{\mathrm{decay},i}$ and σ_i express the decay time from excited state to ground state and the excitation cross section of each Eu^{3+} center, respectively. Under steady-state conditions ($\mathrm{d}N^*_{\mathrm{Eu},i}/\mathrm{d}t = 0$), Eq. (1) yields

$$N^*_{\mathrm{Eu},i} = \frac{\sigma_i\phi}{\sigma_i\phi + \tau^{-1}_{\mathrm{decay},i}} N_{\mathrm{Eu},i}. \tag{2}$$

Thus, the PL intensity from each luminescent center is given by

$$I_i \propto \frac{N^*_{\mathrm{Eu},i}}{\tau_{\mathrm{decay},i}}, \tag{3}$$

where $\tau_{\mathrm{rise},i}$ means rise time of an emission after an excitation for each Eu^{3+} center and can be expressed as[45]

$$\frac{1}{\tau_{\mathrm{rise},i}} = \sigma_i\phi + \frac{1}{\tau_{\mathrm{decay},i}}. \tag{4}$$

From Eqs. (2), (3) and (4), we obtain the concentration of each Eu center expressed as

$$N_{\mathrm{Eu},i} \propto \frac{\tau^2_{\mathrm{decay},i}}{\tau_{\mathrm{decay},i} - \tau_{\mathrm{rise},i}} I_i. \tag{5}$$

$\tau_{\mathrm{rise},i}$ and $\tau_{\mathrm{decay},i}$ for each luminescent center obtained by TR-PL measurements at an excitation power density of 1.7 kW/cm^2 are given in Tab. I (see Sect. I in the supplementary material). Especially for the OMVPE4, the decay time was long because it is associated with Eu^{3+} ions occupying isolated Ga-sites with high symmetry. Higher symmetry typically correlates with long decay times because the crystal field perturbation that breaks the selection rules is weak compared with more complex, lower-symmetry defect sites like OMVPE7[27]. Note that the photo-excitation efficiency of the OMVPE4 under resonant excitation is not remarkably low because the long rise time partly affected by the long decay time as shown in Eq. (4).

The concentration of each luminescent center detected in Figs. 2(a) and (b) was calculated using Eq. (5) as shown in Fig. 3. Instead of the disappeared OMVPE1 and OMVPE2, the other luminescent centers were increased in the (20$\bar{2}$1) GaN:Eu with respect to those in the (0001) GaN:Eu,O. In particular, the amounts of OMVPE7 and OMVPE8 in the (20$\bar{2}$1) GaN:Eu dramatically increased by factors of 139 and 53, respectively.

To clarify the possible reasons leading such considerable variations in the distributions of the luminescent centers, we begin to consider the differences that may arise during the growth processes between the two samples as follows. During the epitaxy, long migration length of Eu adatoms may suppress Eu-clustering because a post-annealing process at 1100°C has been effective to decrease OMVPE1 and OMVPE2[46]. However, the optimal growth temperature of (20$\bar{2}$1) GaN:Eu was lower than that of (0001) GaN:Eu,O by 60°C as we described above, and the growth temperature difference is not the reason for the variation. According to x-ray diffraction measurements, threading dislocation densities (TDDs) of the (20$\bar{2}$1) GaN:Eu and (0001) GaN:Eu,O were estimated to 1.8×10^{8} cm^{-2} and 5.4×10^{8} cm^{-2}, respectively. Although the crystal quality was slightly better in (20$\bar{2}$1) GaN:Eu due to selective area growth of the template layer[47], we consider that it should not be a dominant reason for the variations. This is because low TDD has hardly affected the amount of OMVPE1,2 and has slightly decreased OMVPE7 even for (0001) GaN:Eu,O grown on GaN substrate (TDD $< 6\times10^{8}$ cm^{-2}) in the previous work[40]. While the strain difference, as we mentioned above, may change the number of OMVPE7, it would not be a main reason for the variations in this paper because the density variation ratio caused by the strain has been only 1.9 times at most in the (0001) GaN:Eu,O[41].

At this moment, we speculate that the drastic variation in Eu centers was attributed to promoted oxygen incorporation during the growth of (20$\bar{2}$1) GaN:Eu. The oxygen concentrations in the (0001) GaN:Eu,O and (20$\bar{2}$1) GaN:Eu assessed by SIMS measurements were 7.5×10^{17} and 4.2×10^{18} cm^{-3}, respectively. It is well known that the incorporated oxygen substitutes nitrogen sites (O_N) in GaN and act as donors. Thus, there is a possibility that Fermi-level rose during the growth of (20$\bar{2}$1) GaN:Eu. First-principles calculations have shown that higher Fermi-level decreases the formation energy of Ga-vacancy (V_{Ga}) or the related defects whereas that of Eu^{3+} ions substituting Ga sites (Eu_{Ga}) is constant[48]. Although the formation energy of Eu_{Ga} still remains low compared with that of V_{Ga}, the energy difference dramatically decreases in the (20$\bar{2}$1) GaN:Eu and it may suppress Eu-clustering. In addition, OMVPE7 and OMVPE8 have been considered to have the same local environment involving a V_{Ga}-O_N complex or a V_{Ga} with different charge states[49]. Therefore, the absence of OMVPE1 and OMVPE2 and the drastic increase of OMVPE7 and OMVPE8 may be ascribed to enhanced oxygen incorporation during the growth of (20$\bar{2}$1) GaN:Eu though further investigations such as positron annihilation spectroscopy should be needed.

Subsequently, by comparing PL spectra under resonant and above-bandgap excitations, we investigated the energy transfer efficiency of each Eu luminescent center. From the concentration and the decay time of each luminescent center, the emission spectrum when all the Eu^{3+} ions are homogeneously excited can be expressed as follows,

$$I_{\mathrm{all}}(E)=\sum_i\left(\frac{I_{\mathrm{res},i}(E)}{\int I_{\mathrm{res},i}(E)\,\mathrm{d}E}\frac{N_{\mathrm{Eu},i}}{\tau_{\mathrm{decay},i}}\right), \tag{6}$$

where E and $I_{\mathrm{res},i}(E)$ are the photon energy of emissions and PL intensity of each Eu^{3+} center under resonant excitation, respectively. Combinational analyses of $I_{\mathrm{all}}(E)$ and PL spectrum under above bandgap excitation [$I_{\mathrm{abg}}(E)$] allows to characterize the excitation efficiency of each Eu center mediated by the GaN host. Particularly for the low-temperature spectroscopy, it is possible to distinguish emission from each luminescent center because the each line-width is less than 0.5 meV at 10 K. We defined the ratio of these intensities as excitation efficiency mediated by the GaN host as follows,

$$\eta_i=\frac{I_{\mathrm{abg}}\left(E_{\mathrm{peak},i}\right)}{I_{\mathrm{all}}\left(E_{\mathrm{peak},i}\right)}. \tag{7}$$

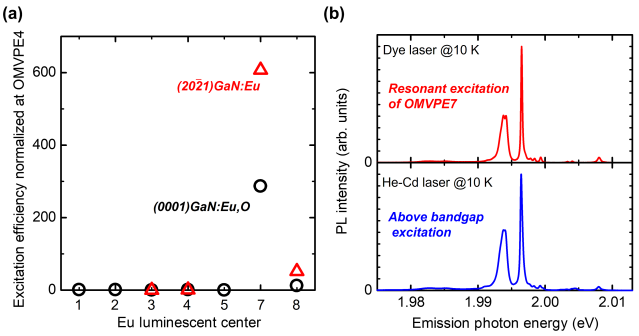

FIG. 4. (a) Excitation efficiency of Eu luminescent centers of (20$\bar{2}$1) GaN:Eu and (0001) GaN:Eu,O under above bandgap excitation at 10 K. (b) PL spectra of (20$\bar{2}$1) GaN:Eu under the resonant excitation of OMVPE7 and under above bandgap excitation at 10 K.

Figure 4(a) shows the relative energy transfer efficiency of each luminescent center normalized by that of the OMVPE4. It was found that the energy transfer efficiencies of the OMVPE7 were about 300 and 600 times higher than those of the OMVPE4 for (0001) GaN:Eu,O and (20$\bar{2}$1) GaN:Eu, respectively. Thus, the energy of injected carriers in host GaN is more likely to transfer to OMVPE7 in (20$\bar{2}$1) GaN:Eu due to the increased concentration, and it means that emission ratio of the OMVPE7 to OMVPE4 is twice as high as in the (0001) GaN:Eu,O under weak excitation conditions. As a result, PL spectrum at 10 K under above-bandgap excitation corresponded well with that under resonant excitation of the OMVPE7 as shown in Fig. 4(b). Note that the excitation efficiency of the OMVPE8 was not considerably high in spite of the drastic increase in the amount for the (20$\bar{2}$1) GaN:Eu. This is because the OMVPE8 is a charged state of the same local atomic structure of the OMVPE7 and shows low luminescence intensity at a cryogenic temperature[50,51], whereas the intensity increases with elevating temperature.

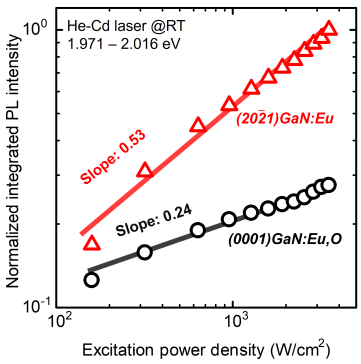

FIG. 5. PL intensities as a function of excitation power of (20$\bar{2}$1) GaN:Eu and (0001) GaN:Eu,O.

Figure 5 shows PL intensities of the samples at RT under above-bandgap excitation integrated from 1.971 eV to 2.016 eV as a function of excitation power density. In general, the luminescent centers with high energy transfer efficiency such as OMVPE7 tend to be preferentially excited even under weak excitation conditions, and therefore the efficiency-droop due to saturation of the emission intensity remarkably occurs under strong excitation conditions. In the (20$\bar{2}$1) GaN:Eu, however, it was found that the efficiency-droop was rather suppressed than that in the (0001) GaN:Eu,O in the range of excitation power density used in this study. This is possibly because the total amount of OMVPE7 and OMVPE8 with high energy transfer rates in the (20$\bar{2}$1) GaN:Eu reached 1.0×10^{19} cm^{-3}, which was comparable to OMVPE4 concentration in (0001) GaN:Eu,O, resulting in the steady-state carrier concentrations in the GaN host at the same excitation power density was reduced. Furthermore, the OMVPE4 itself has also increased by 2.0 times compared in (0001) GaN:Eu,O, and these factors well suppress the efficiency-droop in (20$\bar{2}$1) GaN:Eu.

In summary, we characterized the luminescence properties of the OMVPE-grown (0001) GaN:Eu,O and (20$\bar{2}$1) GaN:Eu. The CEES measurements clarified that the concentrations of OMVPE7 and OMVPE8 in the (20$\bar{2}$1) GaN:Eu were drastically increased by factors of 139 and 53, respectively, due to suppression of Eu clustering and promoted oxygen incorporation. As a result, emissions from (20$\bar{2}$1) GaN:Eu dominated by highly efficient OMVPE7 even under above-bandgap excitation conditions. In addition to the enhanced emission at weak excitations, the increased optically-active luminescent centers well suppressed efficiency-droop even for highly excited conditions, resulting in a 3.6-fold enhancement of emission compared with (0001) GaN:Eu,O at the maximum excitation power density of 3.5 kW/cm^2 used in this study. These results indicate that the growth on (20$\bar{2}$1) GaN is effective method to form efficient Eu luminescent center and will enable to fabricate highly efficient GaN:Eu-based LEDs.

SUPPLEMENTARY MATERIAL

In a supplementary material, we present calculation method of the rise and decay time for each luminescent center. Furthermore, TR-PL profile and fitting results are also described in detail.

ACKNOWLEDGMENTS

This work was supported by JSPS KAKENHI (Grant Nos. 23H05449 and 25K00063) and JST D-Global (Grant No. 24015395).

AUTHOR DECLARATIONS

CONFLICT OF INTEREST

The authors have no conflicts to disclose.

DATA AVAILABILITY

The data that support the findings of this study are available from the corresponding author upon reasonable request.

[1]T. Mukai, M. Yamada, and S. Nakamura, Japanese Journal of Applied Physics **38**, 3976 (1999).
[2]J.-I. Hwang, R. Hashimoto, S. Saito, and S. Nunoue, Applied Physics Express **7**, 071003 (2014).
[3]M. Funato, M. Ueda, Y. Kawakami, Y. Narukawa, T. Kosugi, M. Takahashi, and T. Mukai, Japanese Journal of Applied Physics **45**, L659 (2006).
[4]T. Takeuchi, H. Takeuchi, S. Sota, H. Sakai, H. A. Hiroshi Amano, and I. A. Isamu Akasaki, Japanese Journal of Applied Physics **36**, L177 (1997).
[5]K. Kishino, K. Nagashima, and K. Yamano, Applied Physics Express **6**, 012101 (2012).
[6]Z. Zhuang, D. Iida, and K. Ohkawa, Japanese Journal of Applied Physics **61**, SA0809 (2021).
[7]J. Day, J. Li, D. Y. C. Lie, C. Bradford, J. Y. Lin, and H. X. Jiang, Applied Physics Letters **99**, 031116 (2011).
[8]K. Kishino, N. Sakakibara, K. Narita, and T. Oto, Applied Physics Express **13**, 014003 (2019).
[9]Z. Zhuang, D. Iida, and K. Ohkawa, Applied Physics Letters **116**, 173501 (2020).
[10]S. Ichikawa, K. Shiomi, T. Morikawa, D. Timmerman, Y. Sasaki, J. Tatebayashi, and Y. Fujiwara, Applied Physics Express **14**, 031008 (2021).
[11]T. Takeuchi, S. Sota, M. Katsuragawa, M. Komori, H. Takeuchi, H. A. Hiroshi Amano, and I. A. Isamu Akasaki, Japanese Journal of Applied Physics **36**, L382 (1997).
[12]M. Buongiorno Nardelli, K. Rapcewicz, and J. Bernholc, Applied Physics Letters **71**, 3135 (1997).
[13]R. Singh, D. Doppalapudi, T. D. Moustakas, and L. T. Romano, Applied Physics Letters **70**, 1089 (1997).
[14]M. Auf der Maur, A. Pecchia, G. Penazzi, W. Rodrigues, and A. Di Carlo, Phys. Rev. Lett. **116**, 027401 (2016).
[15]D.-g. Lee, Y. Choi, S. Jung, Y. Kim, S. Park, P. Choi, and S. Yoon, Applied Physics Letters **124**, 121109 (2024).
[16]D. Iida, Z. Zhuang, P. Kirilenko, M. Velazquez-Rizo, M. A. Najmi, and K. Ohkawa, Applied Physics Letters **116**, 162101 (2020).
[17]Y.-M. Huang, C.-Y. Peng, W.-C. Miao, H. Chiang, T.-Y. Lee, Y.-H. Chang, K. J. Singh, Z. D. Iida, R.-H. Horng, C.-W. Chow, C.-C. Lin, K. Ohkawa, S.-C. Chen, and H.-C. Kuo, Photon. Res. **10**, 1978 (2022).

[18]T. Saito, N. Hasegawa, K. Imura, Y. Suehiro, T. Takeuchi, S. Kamiyama, D. Iida, K. Ohkawa, and M. Iwaya, Applied Physics Express **16**, 084001 (2023).
[19]K. Goshonoo, K. Okuno, and M. Ohya, Applied Physics Express **18**, 022003 (2025).
[20]M. S. Wong, D. Hwang, A. I. Alhassan, C. Lee, R. Ley, S. Nakamura, and S. P. DenBaars, Opt. Express **26**, 21324 (2018).
[21]M. S. Wong, J. Back, D. Hwang, C. Lee, J. Wang, S. Gandrothula, T. Margalith, J. S. Speck, S. Nakamura, and S. P. DenBaars, Applied Physics Express **14**, 086502 (2021).
[22]D. Iida and K. Ohkawa, Semiconductor Science and Technology **37**, 013001 (2021).
[23]A. Nishikawa, T. Kawasaki, N. Furukawa, Y. Terai, and Y. Fujiwara, Applied Physics Express **2**, 071004 (2009).
[24]B. Mitchell, V. Dierolf, T. Gregorkiewicz, and Y. Fujiwara, Journal of Applied Physics **123**, 160901 (2018).
[25]D. D. van der Gon, D. Timmerman, Y. Matsude, S. Ichikawa, M. Ashida, P. Schall, and Y. Fujiwara, Opt. Lett. **45**, 3973 (2020).
[26]N. Woodward, A. Nishikawa, Y. Fujiwara, and V. Dierolf, Optical Materials **33**, 1050 (2011), rare earth doped materials for optical based technologies Symposium K of the 2010 EMRS Spring Meeting.
[27]R. Wakamatsu, D.-g. Lee, A. Koizumi, V. Dierolf, and Y. Fujiwara, Journal of Applied Physics **114**, 043501 (2013).
[28]D. Timmerman, B. Mitchell, S. Ichikawa, J. Tatebayashi, M. Ashida, and Y. Fujiwara, Phys. Rev. Appl. **13**, 014044 (2020).
[29]K. Takahei and A. Taguchi, Journal of Applied Physics **74**, 1979 (1993).
[30]D.-g. Lee, R. Wakamatsu, A. Koizumi, Y. Terai, and Y. Fujiwara, Japanese Journal of Applied Physics **52**, 08JM01 (2013).
[31]J. K. Mishra, T. Langer, U. Rossow, S. Shvarkov, A. Wieck, and A. Hangleiter, Applied Physics Letters **102**, 061115 (2013).
[32]B. Mitchell, D. Timmerman, J. Poplawsky, W. Zhu, D. Lee, R. Wakamatsu, J. Takatsu, M. Matsuda, W. Guo, K. Lorenz, E. Alves, A. Koizumi, V. Dierolf, and Y. Fujiwara, Scientific Reports **6**, 18808 (2016).
[33]E. Dumiszewska, W. Strupinski, P. Caban, M. Wesolowski, D. Lenkiewicz, R. Jakiela, K. Pagowska, A. Turos, and K. Zdunek, MRS Online Proceedings Library **1068**, 10680309 (2008).
[34]W. Zhu, B. Mitchell, D. Timmerman, A. Uedono, A. Koizumi, and Y. Fujiwara, APL Materials **4**, 056103 (2016).
[35]S. C. Cruz, S. Keller, T. E. Mates, U. K. Mishra, and S. P. DenBaars, Journal of Crystal Growth **311**, 3817 (2009).
[36]M. Sumiya, K. Yoshimura, K. Ohtsuka, and S. Fuke, Applied Physics Letters **76**, 2098 (2000).
[37]N. Fichtenbaum, T. Mates, S. Keller, S. DenBaars, and U. Mishra, Journal of Crystal Growth **310**, 1124 (2008).
[38]D. A. Browne, E. C. Young, J. R. Lang, C. A. Hurni, and J. S. Speck, Journal of Vacuum Science & Technology A **30**, 041513 (2012).
[39]S. Xu, Y. Hao, J. Zhang, Y. Cao, X. Zhou, L. Yang, X. Ou, K. Chen, and W. Mao, Journal of Crystal Growth **312**, 3521 (2010).
[40]R. Wakamatsu, D.-g. Lee, A. Koizumi, V. Dierolf, Y. Terai, and Y. Fujiwara, Japanese Journal of Applied Physics **52**, 08JM03 (2013).
[41]T. Inaba, B. Mitchell, A. Koizumi, and Y. Fujiwara, Opt. Mater. Express **7**, 1381 (2017).
[42]M. Funato, D. Inoue, M. Ueda, Y. Kawakami, Y. Narukawa, and T. Mukai, Journal of Applied Physics **107**, 123501 (2010).
[43]S. Ichikawa, M. Funato, and Y. Kawakami, Semiconductor Science and Technology **36**, 085016 (2021).
[44]F. Priolo, G. Franzò, S. Coffa, and A. Carnera, Phys. Rev. B **57**, 4443 (1998).
[45]S. Coffa, G. Franzo, and F. Priolo, Applied Physics Letters **69**, 2077 (1996).
[46]T. Iwaya, S. Ichikawa, D. Timmerman, J. Tatebayashi, and Y. Fujiwara, Applied Physics Letters **122**, 032102 (2023).
[47]J. Song, J. Choi, C. Zhang, Z. Deng, Y. Xie, and J. Han, ACS Applied Materials & Interfaces **11**, 33140 (2019).
[48]K. Hoang, Phys. Rev. Mater. **5**, 034601 (2021).
[49]B. Mitchell, J. Poplawsky, D. Lee, A. Koizumi, Y. Fujiwara, and V. Dierolf, Journal of Applied Physics **115**, 204501 (2014).
[50]R. Wakamatsu, D. Timmerman, D. Lee, A. Koizumi, and Y. Fujiwara, Journal of Applied Physics **116**, 043515 (2014).
[51]B. Mitchell, N. Hernandez, D. Lee, A. Koizumi, Y. Fujiwara, and V. Dierolf, Phys. Rev. B **96**, 064308 (2017).